A glutamate/aspartate switch controls product specificity in a protein arginine methyltransferase

Erik W. Debler[a,b,1], Kanishk Jain[c], Rebeccah A. Warmack[c], You Feng[c], Steven G. Clarke[c], Günter Blobel[a,b,1], and Pete Stavropoulos[a,b,d,1]

[a]Laboratory of Cell Biology, The Rockefeller University, New York, NY 10065; [b]Howard Hughes Medical Institute, The Rockefeller University, New York, NY 10065; [c]Department of Chemistry and Biochemistry and The Molecular Biology Institute, University of California, Los Angeles, CA 90095; and [d]Laboratory of Lymphocyte Biology, The Rockefeller University, New York, NY 10065

Contributed by Günter Blobel, January 10, 2016 (sent for review December 18, 2015; reviewed by Gino Cingolani and Laurie K. Read)

***Trypanosoma brucei* PRMT7 (*Tb*PRMT7) is a protein arginine methyltransferase (PRMT) that strictly monomethylates various substrates, thus classifying it as a type III PRMT. However, the molecular basis of its unique product specificity has remained elusive. Here, we present the structure of *Tb*PRMT7 in complex with its cofactor product *S*-adenosyl-L-homocysteine (AdoHcy) at 2.8 Å resolution and identify a glutamate residue critical for its monomethylation behavior. *Tb*PRMT7 comprises the conserved methyltransferase and β-barrel domains, an N-terminal extension, and a dimerization arm. The active site at the interface of the N-terminal extension, methyltransferase, and β-barrel domains is stabilized by the dimerization arm of the neighboring protomer, providing a structural basis for dimerization as a prerequisite for catalytic activity. Mutagenesis of active-site residues highlights the importance of Glu181, the second of the two invariant glutamate residues of the double E loop that coordinate the target arginine in substrate peptides/proteins and that increase its nucleophilicity. Strikingly, mutation of Glu181 to aspartate converts *Tb*PRMT7 into a type I PRMT, producing asymmetric dimethylarginine (ADMA). Isothermal titration calorimetry (ITC) using a histone H4 peptide showed that the Glu181Asp mutant has markedly increased affinity for monomethylated peptide with respect to the WT, suggesting that the enlarged active site can favorably accommodate monomethylated peptide and provide sufficient space for ADMA formation. In conclusion, these findings yield valuable insights into the product specificity and the catalytic mechanism of protein arginine methyltransferases and have important implications for the rational (re)design of PRMTs.**

crystal structure | enzyme catalysis | PRMT | histone methylation | epigenetics

Posttranslational modifications of proteins can affect their structure, catalytic activity, and molecular interactions (1). Methylation of the guanidino group of arginine residues represents a prominent subset of these reactions (2). Histone arginine methylation is associated with gene silencing and activation (3); the modification of arginine residues in a variety of nonhistone proteins, including splicing and transcription factors, can regulate their activity (4, 5).

Most of the enzymes that catalyze arginine methylation are designated protein arginine methyltransferases (PRMTs) and require the cofactor *S*-adenosyl-L-methionine (AdoMet) as the methyl donor (6). Four types of arginine methylation products have been described: ω-N^G-monomethylarginine (MMA), asymmetric ω-N^G-N^G-dimethylarginine (ADMA), symmetric ω-N^G-$N^{G'}$ dimethylarginine (SDMA), and δ-N^G-monomethylarginine (6, 7). Accordingly, PRMTs can be categorized into four groups: Type I PRMTs catalyze ADMA formation, type II PRMTs catalyze SDMA formation, type III PRMTs catalyze MMA formation, and type IV PRMTs catalyze δ-N^G-monomethylarginine formation. Type I, II, and III PRMTs are widely distributed in nature whereas type IV PRMTs seem to be limited to yeasts and plants (8). Interestingly, whereas type I and II enzymes catalyze MMA production in addition to their dimethyl products, type III enzymes are the only PRMTs that produce MMA alone. To date, only one methyltransferase, PRMT7, has been reported to have type III activity in mice, humans, and trypanosomes (9–13). The function of PRMT7 has been linked to cancer metastasis (4, 14, 15), DNA damage (16), pluripotency (17), and parasite infection (18).

All PRMTs that have been structurally characterized to date share a conserved catalytic core of about 300–350 residues constituting an AdoMet-binding methyltransferase and a β-barrel domain. Another common feature of PRMTs is the dimerization of the catalytic core that is realized in most cases by noncovalent association of two protomers. Covalent linkage of two PRMT modules has also been observed (19–22). Although representative structures of type I, II, and III enzymes have been determined (13, 19, 20, 23–25), our understanding of product specificity in these enzymes remains fragmentary. To unravel the molecular basis of the strict MMA activity of PRMT7 enzymes, we determined the X-ray crystal structure of *Trypanosoma brucei* PRMT7 (*Tb*PRMT7), which was recently reported in two different crystal forms (13). Although this former study established its dimeric state in solution (13), we generated a dimerization-deficient mutant where active-site residues remain intact and demonstrated that dimerization is necessary for catalysis. Importantly, we performed extensive mutational analysis and identified and proved for the first time, to our knowledge, that Glu181 is a key residue for monomethylation by *Tb*PRMT7. We carried out isothermal titration calorimetry (ITC) to characterize peptide binding to WT and mutant proteins and assayed product formation. Collectively, these studies provide new insights into the catalytic mechanism and product specificity of this class of enzymes.

Significance

Posttranslational modifications in proteins profoundly modulate their function, and enzymes that generate these modifications therefore have key regulatory roles in a wide array of biological processes. Protein arginine methyltransferases (PRMTs) attach methyl group(s) to arginines and differ in their product specificity, as they form either monomethyl arginine (MMA), asymmetric dimethylarginine (ADMA), or symmetric dimethylarginine (SDMA), each of which relays specific biological signals. Although the members of the PRMT family are structurally highly homologous, the precise molecular basis of their product specificity has not been determined. Based on our structure of *Tb*PRMT7, which explicitly forms MMA, we identified a glutamate residue as a key determinant of its product specificity, and we were able to engineer a *Tb*PRMT7 mutant capable of ADMA formation.

Author contributions: E.W.D., S.G.C., G.B., and P.S. designed research; E.W.D., K.J., R.A.W., Y.F., and P.S. performed research; E.W.D., K.J., R.A.W., Y.F., S.G.C., G.B., and P.S. analyzed data; and E.W.D., K.J., R.A.W., S.G.C., and P.S. wrote the paper.

Reviewers: G.C., Thomas Jefferson University; and L.K.R., University at Buffalo.

The authors declare no conflict of interest.

Data deposition: The atomic coordinates and structure factors have been deposited in the Protein Data Bank, www.pdb.org (PDB ID code 5EKU).

[1]To whom correspondence may be addressed. Email: edebler@rockefeller.edu, blobel@rockefeller.edu, or stavrop@rockefeller.edu.

This article contains supporting information online at www.pnas.org/lookup/suppl/doi:10.1073/pnas.1525783113/-/DCSupplemental.

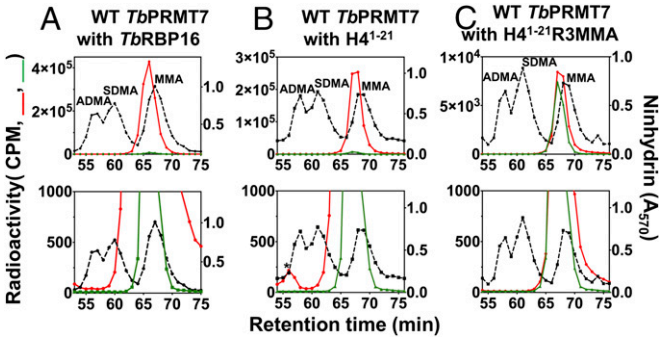

Fig. 1. *Tb*PRMT7 displays Type III PRMT activity. *Tb*PRMT7 was incubated with [*methyl*-^{3}H]-AdoMet and (*A*) *Tb*RBP16; (*B*) an *N*-acetyl peptide corresponding to residues 1–21 of human histone H4 ($H4^{1-21}$); or (*C*) the $H4^{1-21}$ peptide with MMA substituted for arginine at position 3 ($H4^{1-21}$R3MMA). Protein or peptides from the incubation were hydrolyzed and mixed with amino acid standards of ADMA, SDMA, and MMA and then analyzed via high-resolution cation-exchange chromatography. The red lines indicate the radioactivity of ^{3}H-methyl groups for complete reactions. The green lines indicate the radioactivity from a single control reaction where the enzyme alone was incubated with [*methyl*-^{3}H]-AdoMet as an automethylation control and is shown in each panel. The elution of the amino acid standards was determined by ninhydrin reactivity and is shown as a black dashed line. In each case, *Lower* represents an enlargement to show lower levels of methylation. Isotopically labeled ADMA, SDMA, and MMA elute about a minute earlier than the nonisotopically labeled standards due to the effect of tritium on the pK_as of the methylarginine species (11, 32). The asterisked small radioactive peak in *B*, *Lower* migrates about 1 min earlier than expected for [^{3}H]ADMA—the identity of this material is unknown.

Results

***Tb*PRMT7 Is a Type III PRMT That Forms only Monomethylarginine.** *Tb*PRMT7 exclusively produces MMA with protein substrates including histones and trypanosomal RNA binding protein 16 (*Tb*RBP16) (12). *Tb*PRMT7 also effectively methylates a peptide corresponding to the amino acid sequence of the 21 N-terminal residues of human histone H4; however, when the arginine residue at position 3 was replaced by an MMA residue, little or no methylation was observed (13), suggesting that Arg-3 was the prominent site of methylation in this peptide and that the enzyme was unable to catalyze the addition of a second methyl group on this residue to form SDMA or ADMA. However, the sensitivity of the latter assay was low.

To rule out any possible dimethylation, we used *Tb*RBP16 and human histone H4 peptides (residues 1–21) as substrates in an amino acid analysis method that could detect specific dimethylated substrates on a subfemtomole level. We were able to demonstrate the complete inability of *Tb*PRMT7 to produce dimethylarginine species with *Tb*RBP16 under conditions where 0.01% of such methylated species would be detected (Fig. 1*A*); sensitivity is based on the ratio of the background radioactivity to the MMA peak radioactivity. We next demonstrated that a histone $H4^{1-21}$ peptide acetylated at its N terminus is also an excellent substrate for *Tb*PRMT7 and yields only MMA where 0.02% of a dimethylated product would be detected (Fig. 1*B*). Finally, we were able to directly test for dimethylation using the corresponding peptide that had MMA substituted for arginine at position 3 ($H4^{1-21}$R3MMA); the presence of only monomethylated H4 peptide provides a direct substrate for any dimethylation reaction and limits any competition for methylation between unmethylated and monomethylated species. Again, no production of dimethylated arginine species was detected under conditions where 0.5% would be readily detected (Fig. 1*C*). Only a small increase in MMA over the background of automethylation was observed (perhaps due to methylation at arginine-17 and/or arginine-19), indicating that the major site of methylation on this peptide is at arginine-3 (Fig. 1*C*).

Overall Structure of *Tb*PRMT7. To obtain a detailed picture of the active site at atomic resolution, we set out to determine the X-ray crystal structure of *Tb*PRMT7. Limited proteolysis on the full-length protein identified a stable, N-terminally truncated fragment spanning residues 32–390, referred to as *Tb*PRMT7 in the remainder of the text for convenience. Notably, its catalytic activity is comparable with that of the full-length protein. To obtain phase information for the de novo structure determination, the protein was derivatized with seleno-methionine. The 2.8-Å crystal structure was solved using the single anomalous dispersion (SAD) phasing technique and refined to an R_{free}/R_{work} = 26.1/22.1%. For details of the data collection and refinement statistics, see Table S1.

In an independent study, Wang et al. identified a similar core fragment of *Tb*PRMT7 (residues 36–378) and determined its crystal structure in two different crystal forms (13). Despite the alternative crystal packing, *Tb*PRMT7 adopts the same compact, roughly rhombus-shaped homodimer, in which two protomers are arranged in an antiparallel fashion with a twofold symmetry axis perpendicular to the rhombus (Fig. 2*B*) (13). Because the dimeric *Tb*PRMT7–*S*-adenosyl-L-homocysteine (AdoHcy) complexes are essentially identical in the different crystal forms with an rmsd of 0.5 Å for 670 Cα atoms, confirming the validity of the

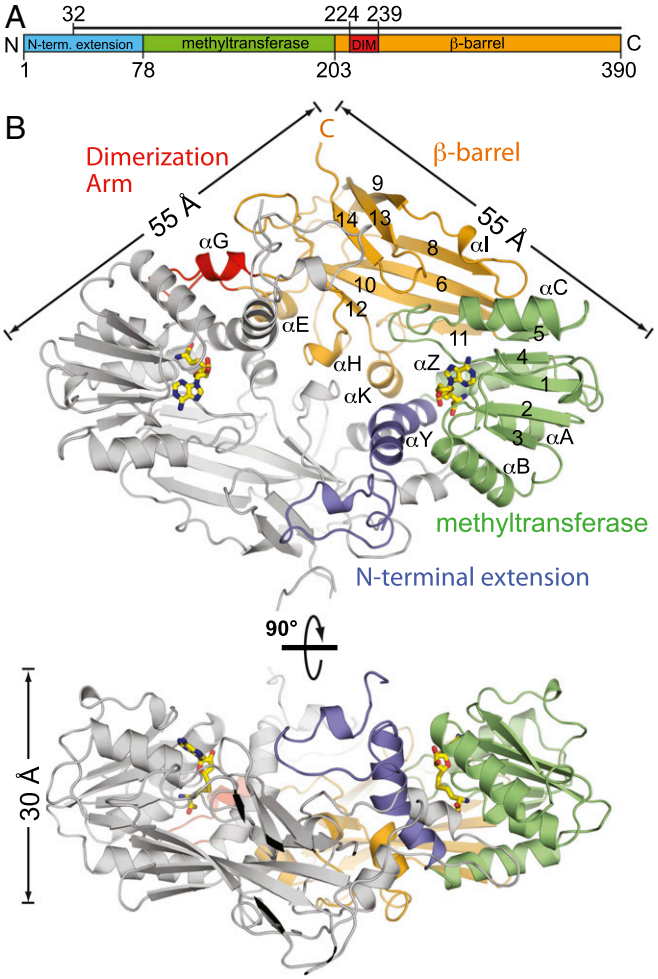

Fig. 2. Overview of *Tb*PRMT7 in complex with AdoHcy. (*A*) Domain organization of *Tb*PRMT7. Domain boundaries are indicated by residue numbers. The bar above the domain structure denotes the crystallized fragment. DIM, dimerization arm. (*B*) Ribbon representation of the *Tb*PRMT7 dimer, using the same color code for the domains as in *A*. The second protomer of the *Tb*PRMT7 dimer is shown in gray. AdoHcy is displayed in yellow stick representation. (*Lower*) A 90° rotated view is shown. Labeling of α-helices and β-strands follows the convention of earlier structures (23, 24).

Table 1. Type III enzymatic activity of WT and mutant *Tb*PRMT7 enzymes

Enzyme	Percentage type III activity
WT	100
Automethylation	1.3
Dimerization mutants	
224–235 mutated to 12 glycines	0.16
1–74 deletion	0.0055
Double E loop mutants	
G180Y	119
I173L F174L	109
I173V	102
G180N	58
E172D	21
E181D	14.2
I173A	8.6
I173G	1.9
E181Q	1.1
E172D E181D	0.32
E172Q	0.17
I173P F174M	0.04
G175D M177E	0.02
THW motif mutants	
Q329H	99.6
Q329F	90.1
Q329A	14.1
W330A	46
Helix αY mutants	
F71A	96.1
M75F	94.5
M75A	5.2

dimeric structure, only key features of the overall structure are recapitulated below.

The structured core of a *Tb*PRMT7 protomer resembles that of other PRMTs and consists of four modules: an N-terminal extension (residues 32–77), the AdoHcy-containing methyltransferase domain (residues 78–202), and the β-barrel domain (residues 203–390) that contains a protruding dimerization arm (residues 224–238) (Fig. 2*B*) (13, 23, 24). The two active sites that would bind the methyl donor AdoMet and the target arginine of the substrate are located ∼36 Å apart on the same face of the homodimer. The total buried surface area between the two protomers amounts to 7,560 Å^2 as calculated by the PISA server (26) and is primarily formed by the N-terminal extension and the dimerization arm and to a smaller degree by helices αE, αH′, and αK at the center of the dimer (Fig. 2*B*).

Dimerization Is Necessary for *Tb*PRMT7 Catalytic Activity. Using multi-angle light scattering (MALS), we confirmed that *Tb*PRMT7 exists as a dimer in solution (Fig. S1), consistent with the large interface observed in the crystal structure and consistent with previous results from small-angle X-ray scattering (13). To assess the importance of dimerization for catalysis, we created a mutant that is deficient in dimerization while keeping the active site intact. To this end, we replaced residues 224–235 of the dimerization arm with glycines. This dimerization arm mutant was exclusively monomeric in solution, indicating that the mutant is still properly folded whereas its catalytic activity was greatly reduced (Table 1). These data strongly suggest a requirement of dimerization for efficient catalysis. We confirmed this correlation with a second mutant, in which the N-terminal extension (residues 1–74 including helix αY) was truncated. Again, dimerization is abolished with a concomitant loss in catalytic activity (Table 1). However, because helix αY of the N-terminal extension directly contributes several residues to the active site (Fig. 3), the effect of helix αY removal cannot be solely ascribed to the dimerization deficiency.

Active Site of *Tb*PRMT7. The active site of *Tb*PRMT7 is formed by the methyltransferase domain, helix αY in the N-terminal extension, and a short motif of the β-barrel (Fig. 3). The cofactor product AdoHcy is well-defined in the electron density map, adopts its canonical conformation observed in AdoMet-dependent methyltransferases, and engages in highly conserved interactions with the methyltransferase domain (24). AdoHcy sits in the lower part of the binding pocket with the methionine moiety at the bottom whereas the upper part of the cavity is poised for accommodating the incoming arginine of the substrate. The strongly negative electrostatic surface potential of the binding pocket is complementary to a substrate harboring a positively charged arginine residue (Fig. S2). Because the methyl group of AdoMet is transferred from its sulfur atom to a terminal nitrogen atom of the target arginine during catalysis, the residues adjacent to the sulfur atom of AdoHcy are expected to be most relevant for governing product specificity in *Tb*PRMT7. The two conserved eponymous glutamate residues, Glu172 and Glu181, as well as Ile173 of the double E loop in the methyltransferase domain, form one side of the binding pocket (27), opposed by Phe71 and His72 of helix αY in the N-terminal extension on the other side. The bottom of the pocket is formed by Met75 of helix αY whereas Gln329 and Trp330 of helix αK in the β-barrel domain are wedged between the methyltransferase domain and the N-terminal extension. The latter two residues are part of the THW motif termed after the threonine, histidine, and tryptophan residues predominantly found in type I PRMTs. In PRMT7 enzymes, however, methionine and glutamine substitute for the threonine and histidine residues. Comparison with the *Tb*PRMT7–AdoHcy complex of another crystal form (PDB ID code 4M37) reveals that almost all active-site residues adopt identical positions and rotamers, with slight deviations observed for Met75, Glu172, Glu181, and Gln329.

Active-Site Mutations Decrease Type III Methylation Activity. To investigate the impact of individual residues on the methylation activity, mutations were made at key residues in the active site: e.g., the double E loop and THW motif (27). Using *Tb*RBP16 as a substrate, MMA production was assayed by amino acid analysis (Table 1). Several of the mutants displayed similar levels of MMA as WT *Tb*PRMT7, including mutants for three residues in the double E loop (Ile173Val, Ile173Leu/Phe174Leu, and Gly180Tyr), a mutant of the THW motif (Gln329His), and two mutants in helix αY (Phe71Ala and Met75Phe). Although these mutations did not markedly affect activity, the remaining mutants displayed severe losses in activity, highlighting the significance of these residues in catalysis. Notably, no ADMA or

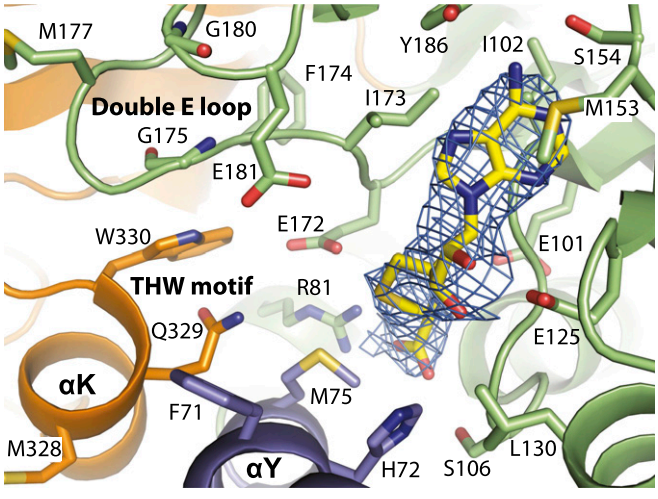

Fig. 3. Active site of *Tb*PRMT7. The electron density of AdoHcy and key residues in the active site are shown.

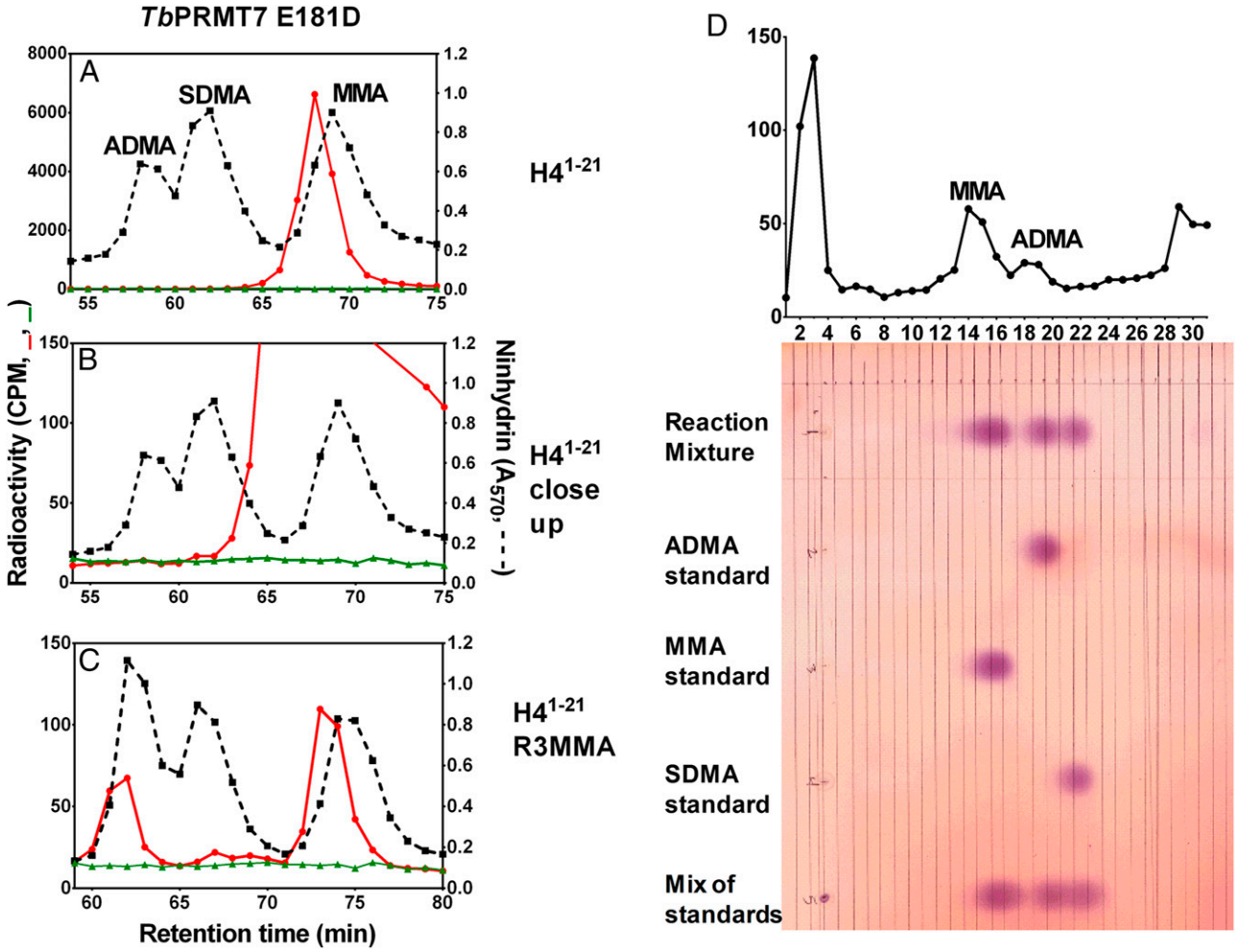

Fig. 4. An active-site mutation in the double E loop of *Tb*PRMT7 produces ADMA. *Tb*PRMT7 Glu181Asp was incubated with [*methyl*-^{3}H]-AdoMet and (*A* and *B*) the H4$^{1-21}$ peptide or (*C* and *D*) the H4$^{1-21}$R3MMA peptide. Hydrolysates of the peptide products were mixed with amino acid standards of ADMA, SDMA, and MMA and were analyzed via high-resolution cation exchange chromatography (*A*–*C*) or TLC (*D*). Red lines in *A*–*C* indicate the radioactivity of ^{3}H-*methyl* groups for complete reactions. The green lines indicate the radioactivity from a single control reaction where the enzyme alone was incubated with [*methyl*-^{3}H]-AdoMet as an automethylation control and is shown in each panel. (*B*) An enlargement of the radioactive data in *A*. The elution of the amino acid standards was determined by a ninhydrin reaction, shown in black dashes. Isotopically labeled ADMA and MMA elute about a minute earlier than the nonisotopically labeled standards. (*D*) TLC for hydrolysates of the reaction mixture and individual and mixed standards of ADMA, MMA, and SDMA. (*Upper*) The radioactivity corresponding to the TLC slices of the reaction mixture lane. (*Lower*) The ninhydrin staining of the TLC plate.

SDMA product was formed in any of these mutants under conditions where 0.02% would have been detected.

A Mutation in the Double E Loop Converts *Tb*PRMT7 into an ADMA-Producing Enzyme. The ability of PRMTs to dimethylate arginines to form either SDMA or ADMA relies on sufficient space within the active site to accommodate not only the unmodified but also the larger monomethylated arginine residue for subsequent dimethylation (28). Notably, none of the mutants yielded any ADMA or SDMA with *Tb*RBP16 or the H4$^{1-21}$ peptide. Many of these mutants showed significantly decreased activity, making it difficult to observe any level of possible dimethylarginine products. To overcome this limitation, the activity of certain mutants was tested with an already methylated H4 peptide at Arg3 (H4$^{1-21}$R3MMA). When H4$^{1-21}$R3MMA is used as a substrate with mutant Glu181Asp, we demonstrated production of both MMA and ADMA (Fig. 4*C*). The MMA formed here presumably results from the methylation of the unmodified arginine-17 and/or arginine-19 residues. With the unmodified H4$^{1-21}$ peptide, the Glu181Asp mutant shows strictly type III activity (Fig. 4 *A* and *B*).

A similar mutational study of the first glutamate in *Tb*PRMT7's double E loop (Glu172Asp) did not reveal any production of dimethylated arginine species. The side chain carboxyl atoms of the first glutamate residue in the *Tb*PRMT7 double E loop (Glu172) have lower B-values than those of the second glutamate (Glu181), consistent with the deeper burial of Glu172 in the protein interior and its larger number of interactions with neighboring residues than the more solvent-exposed Glu181. A similar situation occurs for the first and second glutamate residues in the double E loop of other PRMTs (Table S2). To further confirm the production of ADMA, TLC was performed with acid hydrolysates of the methylation reaction and methylarginine standards. Radioactivity from TLC slices confirmed that the Glu181Asp mutant does produce both MMA and ADMA with the H4$^{1-21}$R3MMA peptide (Fig. 4*D*).

The *Tb*PRMT7 Glu181Asp Mutant Has a Higher Affinity for the Monomethylated Peptide than WT *Tb*PRMT7. To analyze peptide binding to the WT and mutant Glu181Asp enzymes, we performed isothermal titration calorimetry (ITC) with H4$^{1-21}$ and H4$^{1-21}$ R3MMA peptides (Fig. 5). Consistent with a strong electrostatic interaction, binding of the H4$^{1-21}$ peptide to *Tb*PRMT7 was highly dependent on ionic strength, with relatively strong binding (K_D = 2.7 μM) at low salt concentration (20 mM NaCl) and essentially no binding at 300 mM NaCl (K_D = 0.4 M) (Table S3). The WT

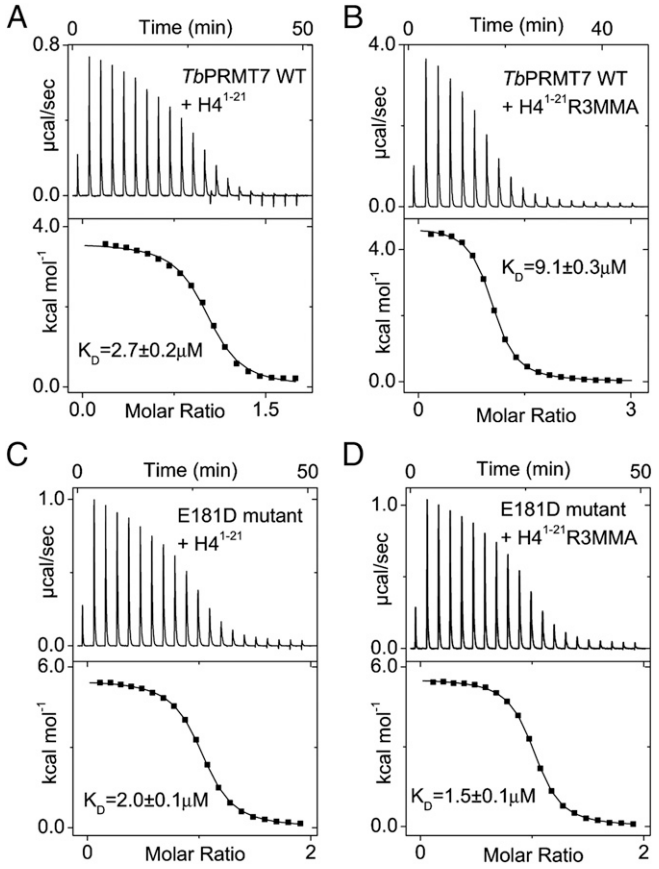

Fig. 5. Isothermal titration calorimetry of *Tb*PRMT7 WT (*A* and *B*) and Glu181Asp mutant (*C* and *D*) with $H4^{1-21}$ and $H4^{1-21}$R3MMA, respectively.

*Tb*PRMT7 enzyme binds its substrate $H4^{1-21}$ with higher affinity (K_D = 2.7 µM) than its monomethylation product $H4^{1-21}$R3MM (K_D = 9.1 µM), thermodynamically favoring product release. Although the affinity for the unmodified $H4^{1-21}$ peptide (K_D = 2.0 µM) is essentially unchanged in the Glu181Asp mutant with respect to the WT enzyme, this mutant strikingly has increased binding affinity for the methylated peptide (K_D = 1.5 vs. 9.1 µM of the WT). Thus, the Glu181Asp mutant favors binding of the bulkier $H4^{1-21}$R3MM peptide, which can be rationalized by providing a more spacious binding pocket, stabilizing the MMA substrate–enzyme interactions and enabling dimethylation.

Discussion

We determined the crystal structure of a protein arginine methyltransferase, PRMT7 from *T. brucei*, in complex with the methyl donor product AdoHcy and performed biochemical and mutational analyses to elucidate its catalytic mechanism and the structural basis of its unique product specificity. Although various suggestions have been made for the role of specific residues in the active site of PRMTs and although a constricted active site has recently been suggested as the basis for MMA activity in different crystal forms of *Tb*PRMT7 (13, 27), little is known experimentally about key residues that direct which methylarginine derivative is produced. This product specificity is crucial to the function of these enzymes because proteins that bind methylated substrates (so-called "methyl readers") differentially recognize ADMA and SDMA (3, 29), and potentially MMA. Thus, defining the exact components of catalysis and product specificity for this class of enzymes has become increasingly important. Although it has not been established that the mammalian and trypanosomal PRMT7 enzymes have the same function, the degree of sequence identity (28% over the full-length *Tb*PRMT7 protein compared with human PRMT7), its strict monomethylating behavior, and its robust enzymatic activity make the protozoan enzyme a facile system to study the biochemistry of type III PRMTs.

Notably, *Tb*PRMT7 and mammalian PRMT7 have a distinct structural organization (9, 10, 13, 20). Although the mammalian enzymes contain two PRMT cores in tandem, the trypanosomal enzyme contains only one PRMT core. However, our light scattering analysis (Fig. S1) as well as previous small-angle X-ray scattering studies (13) showed that *Tb*PRMT7 forms a homodimer in solution. The juxtaposition of the two tandem PRMT cores in mouse and roundworm PRMT7 crystal structures recapitulates the dimeric *Tb*PRMT7 architecture, sharing a similar overall quaternary structure (19, 20). Although only one PRMT module is catalytically active in mouse PRMT7 (*Mm*PRMT7) and roundworm PRMT7 (*Ce*PRMT7) (19, 20), our data (Table 1), as well as those of others, suggest that dimerization of PRMT7 cores—either by a noncovalent assembly or by juxtaposition of two units as part of one polypeptide—is a prerequisite for catalytic activity (19, 20).

Another difference between mammalian and trypanosomal PRMT7 enzymes pertains to their substrate specificity (9, 10, 13, 20). Human PRMT7, for example, has a substrate specificity for RXR motifs surrounded by basic residues, such as Arg17 and Arg19 in $H4^{1-21}$ (9, 10), whereas our experiments with WT *Tb*PRMT7 and the $H4^{1-21}$ peptide demonstrate that arginine methylation does not occur at this motif. By contrast, Arg3 is the major site of methylation in this peptide by *Tb*PRMT7 (Fig. 1), as indicated by the lack of MMA production above automethylation levels with the $H4^{1-21}$ peptide monomethylated at Arg3. Furthermore, the absence of any additional methylated species confirms the inability of *Tb*PRMT7 to catalyze dimethylation reactions.

Site-directed mutagenesis experiments involving residues of the *Tb*PRMT7 active site have given insight into key structural players of this enzyme's function. Several of the mutations are located in known PRMT motifs—including Gln329Ala in the THW motif as well as Glu172Gln and Glu181Gln in the double E loop (13, 27). The importance of the double E loop in determining PRMT activity has been widely reported (27) because the methylated nitrogen atoms of the arginine(s) in substrate proteins are coordinated through these two glutamate residues (13, 24, 25). These results demonstrate the importance of these residues on the activity of the *Tb*PRMT7 enzyme.

By analyzing the effects that certain residues have on *Tb*PRMT7 in a biochemical and structural context, we have identified Glu181 as a crucial molecular component of this enzyme's unique catalysis (Fig. 4). In so doing, we have also expanded the current understanding of how type I and type III enzymes behave and why their methylation behavior differs from one another. A comparison of the distance between the two glutamate residues of the double E loop shows that the glutamates of the type III PRMTs are generally closer together (8.4 Å on average for *Tb*PRMT7, PDB ID codes 4M36, 4M37, 4M38, and 5EKU; 6.8 Å for *Ce*PRMT7, PDB ID codes 3WST and 3XOD; and 8.7 Å for *Mm*PRMT7, PDB ID code 4C4A) than those in type I PRMTs (e.g., 12.5 Å in *Rn*PRMT1, PDB ID code 1ORI; 13.2 Å in *Mm*PRMT6, PDB ID code 4C07; and 8.5 Å in *Hs*PRMT4, PDB ID code 4IKP) (Fig. S3), consistent with the previous finding that *Tb*PRMT7 features a smaller guanidine binding pocket with respect to type I and type II PRMTs (13). The Glu181Asp mutation effectively shortens the side chain at that position by one carbon–carbon bond, increasing the distance between the flanking residues of the double E loop. An enlarged cavity would resemble the larger type I enzyme cavities more closely and allow for the recognition of an already methylated species, resulting in subsequent dimethylation. Indeed, our binding studies show a marked increase in affinity in the Glu181Asp mutant for a methylated substrate ($H4^{1-21}$R3MMA) with respect to the WT enzyme (Fig. 5). The Glu181Asp mutation still maintains the same charge at that position, allowing for similar interactions between the enzyme and the substrate's arginine, albeit at a weaker level. These findings provide a model for predicting the structural determinants of type I methylation, mediated by enzymes with longer distances between glutamates

of the double E loop, versus type III methylation, mediated by enzymes with relatively shorter distances between the glutamates of the double E loop (about 1–2 Å shorter).

Product specificity plays also an important role in histone lysine methyltransferases (HKMTs) because mono-, di-, and trimethylation of lysines relay different biological signals and thus must be strictly controlled. A comparison between the structures of the lysine monomethyltransferase SET7/9 and the trimethyltransferase DIM-5 revealed that the different product specificity can be ascribed to a switch between a tyrosine in SET7/9 for a phenylalanine residue in DIM-5 (30, 31). In detail, DIM-5 contains Phe281 in close proximity to the ε-amino group of the target lysine. In SET7/9, Tyr305 occupies the equivalent position of Phe281 in DIM-5. The addition of the hydroxyl group in Tyr305 narrows the substrate channel and sterically hinders the insertion of a dimethylated ε-amino group at the target lysine, resulting in strict monomethylation activity of SET7/9. Strikingly, the Phe281Tyr mutation in DIM-5 resulted in the alteration of product specificity from a trimethylated lysine to a mono- and dimethylated product whereas the reverse mutation of Tyr305Phe in SET7/9 abolished the strict monomethylation activity and allowed for the formation of di- and trimethylated product. This tyrosine/phenylalanine switch in HKMTs depicts the importance of the absence or presence of a single nonhydrogen atom in the active site for product specificity and recapitulates our finding of an analogous glutamate/aspartate switch that controls product specificity in PRMTs.

In conclusion, our biochemical and structural analyses have defined the components that restrict type III PRMTs to only monomethylate their target arginines and, more generally, have provided insights into the attributes that direct PRMT-mediated catalysis. This knowledge not only will be useful for the prediction of the methylation behavior of novel, thus far uncharacterized members of this family but also will prove valuable in the rational (re)design of other PRMTs.

Methods

The details of molecular cloning, expression, purification, crystallization, X-ray diffraction data collection, structure determination, isothermal titration calorimetry, multiangle light scattering, and amino acid analysis of protein and peptide substrates are described in *SI Methods*. In short, *Tb*PRMT7 was expressed in *E. coli* with an N-terminal His-tag. Recombinant proteins were purified using several chromatographic techniques. The structure was solved by SAD from seleno-L-methionine–labeled crystals.

ACKNOWLEDGMENTS. We thank H. Rust (The Scripps Research Institute) and P. Thompson (UMass Medical School) for providing the $H4^{1-21}$ and $H4^{1-21}$R3MMA peptides, L. Read [State University of New York (SUNY) Buffalo] for providing the expression vector for *Tb*RBP16, M. Dzialo (University of California, Los Angeles) for help with amino acid analysis, D. Berman (Rockefeller University) for help with protein expression and purification, D. King (University of California, Berkeley) for mass spectrometry analysis, M. Becker and R. Fischetti [Advanced Photon Source (APS)] and W. Shi [National Synchrotron Light Source (NSLS)] for support during data collection, and the Structural Biology and the High-Throughput Screening and Spectroscopy Resource Centers at Rockefeller University for support. X-ray data were measured at the GM/CA beamline 23ID-D at APS, supported by funds from the National Cancer Institute (NCI) (Grant ACB-12002) and National Institute of General Medical Sciences (Grant AGM-12006), and at beamline X29 at NSLS, supported by NIH Grants P41GM103473 and P30-EB-00998. E.W.D. was a Frey Fellow of the Damon Runyon Cancer Research Foundation (DRG-1977-08). This work was also supported by grants from NIH, including Grant GM026020 (to S.G.C.) and Ruth L. Kirschstein National Service Award GM007185 (to K.J. and R.A.W.).

1. Walsh G, Jefferis R (2006) Post-translational modifications in the context of therapeutic proteins. *Nat Biotechnol* 24(10):1241–1252.
2. Carr SM, Poppy Roworth A, Chan C, La Thangue NB (2015) Post-translational control of transcription factors: Methylation ranks highly. *FEBS J* 282(23):4450–4465.
3. Dhar SS, et al. (2012) Trans-tail regulation of MLL4-catalyzed H3K4 methylation by H4R3 symmetric dimethylation is mediated by a tandem PHD of MLL4. *Genes Dev* 26(24):2749–2762.
4. Baldwin RM, et al. (2015) Protein arginine methyltransferase 7 promotes breast cancer cell invasion through the induction of MMP9 expression. *Oncotarget* 6(5):3013–3032.
5. Biggar KK, Li SS (2015) Non-histone protein methylation as a regulator of cellular signalling and function. *Nat Rev Mol Cell Biol* 16(1):5–17.
6. Bedford MT, Clarke SG (2009) Protein arginine methylation in mammals: Who, what, and why. *Mol Cell* 33(1):1–13.
7. Herrmann F, Pably P, Eckerich C, Bedford MT, Fackelmayer FO (2009) Human protein arginine methyltransferases in vivo: Distinct properties of eight canonical members of the PRMT family. *J Cell Sci* 122(Pt 5):667–677.
8. Niewmierzycka A, Clarke S (1999) S-Adenosylmethionine-dependent methylation in Saccharomyces cerevisiae: Identification of a novel protein arginine methyltransferase. *J Biol Chem* 274(2):814–824.
9. Feng Y, Hadjikyriacou A, Clarke SG (2014) Substrate specificity of human protein arginine methyltransferase 7 (PRMT7): The importance of acidic residues in the double E loop. *J Biol Chem* 289(47):32604–32616.
10. Feng Y, et al. (2013) Mammalian protein arginine methyltransferase 7 (PRMT7) specifically targets RXR sites in lysine- and arginine-rich regions. *J Biol Chem* 288(52):37010–37025.
11. Zurita-Lopez CI, Sandberg T, Kelly R, Clarke SG (2012) Human protein arginine methyltransferase 7 (PRMT7) is a type III enzyme forming ω-NG-monomethylated arginine residues. *J Biol Chem* 287(11):7859–7870.
12. Fisk JC, et al. (2009) A type III protein arginine methyltransferase from the protozoan parasite Trypanosoma brucei. *J Biol Chem* 284(17):11590–11600.
13. Wang C, et al. (2014) Structural determinants for the strict monomethylation activity by trypanosoma brucei protein arginine methyltransferase 7. *Structure* 22(5):756–768.
14. Yao R, et al. (2014) PRMT7 induces epithelial-to-mesenchymal transition and promotes metastasis in breast cancer. *Cancer Res* 74(19):5656–5667.
15. Yang Y, Bedford MT (2013) Protein arginine methyltransferases and cancer. *Nat Rev Cancer* 13(1):37–50.
16. Karkhanis V, et al. (2012) Protein arginine methyltransferase 7 regulates cellular response to DNA damage by methylating promoter histones H2A and H4 of the polymerase δ catalytic subunit gene, POLD1. *J Biol Chem* 287(35):29801–29814.
17. Wang YC, Peterson SE, Loring JF (2014) Protein post-translational modifications and regulation of pluripotency in human stem cells. *Cell Res* 24(2):143–160.
18. Ferreira TR, et al. (2014) Altered expression of an RBP-associated arginine methyltransferase 7 in Leishmania major affects parasite infection. *Mol Microbiol* 94(5):1085–1102.
19. Hasegawa M, Toma-Fukai S, Kim JD, Fukamizu A, Shimizu T (2014) Protein arginine methyltransferase 7 has a novel homodimer-like structure formed by tandem repeats. *FEBS Lett* 588(10):1942–1948.
20. Cura V, Troffer-Charlier N, Wurtz JM, Bonnefond L, Cavarelli J (2014) Structural insight into arginine methylation by the mouse protein arginine methyltransferase 7: A zinc finger freezes the mimic of the dimeric state into a single active site. *Acta Crystallogr D Biol Crystallogr* 70(Pt 9):2401–2412.
21. Yang Y, et al. (2015) PRMT9 is a type II methyltransferase that methylates the splicing factor SAP145. *Nat Commun* 6:6428.
22. Hadjikyriacou A, Yang Y, Espejo A, Bedford MT, Clarke SG (2015) Unique features of human protein arginine methyltransferase 9 (PRMT9) and its substrate RNA splicing factor SF3B2. *J Biol Chem* 290(27):16723–16743.
23. Weiss VH, et al. (2000) The structure and oligomerization of the yeast arginine methyltransferase, Hmt1. *Nat Struct Biol* 7(12):1165–1171.
24. Zhang X, Zhou L, Cheng X (2000) Crystal structure of the conserved core of protein arginine methyltransferase PRMT3. *EMBO J* 19(14):3509–3519.
25. Sun L, et al. (2011) Structural insights into protein arginine symmetric dimethylation by PRMT5. *Proc Natl Acad Sci USA* 108(51):20538–20543.
26. Krissinel E, Henrick K (2007) Inference of macromolecular assemblies from crystalline state. *J Mol Biol* 372(3):774–797.
27. Fuhrmann J, Clancy KW, Thompson PR (2015) Chemical biology of protein arginine modifications in epigenetic regulation. *Chem Rev* 115(11):5413–5461.
28. Lee HW, Kim S, Paik WK (1977) S-adenosylmethionine: Protein-arginine methyltransferase. Purification and mechanism of the enzyme. *Biochemistry* 16(1):78–85.
29. Migliori V, et al. (2012) Symmetric dimethylation of H3R2 is a newly identified histone mark that supports euchromatin maintenance. *Nat Struct Mol Biol* 19(2):136–144.
30. Xiao B, et al. (2003) Structure and catalytic mechanism of the human histone methyltransferase SET7/9. *Nature* 421(6923):652–656.
31. Zhang X, et al. (2003) Structural basis for the product specificity of histone lysine methyltransferases. *Mol Cell* 12(1):177–185.
32. Gottschling H, Freese E (1962) A tritium isotope effect on ion exchange chromatography. *Nature* 196:829–831.
33. Hayman ML, Read LK (1999) Trypanosoma brucei RBP16 is a mitochondrial Y-box family protein with guide RNA binding activity. *J Biol Chem* 274(17):12067–12074.
34. Otwinowski Z, Minor W (1997) Processing of X-ray diffraction data collected in oscillation mode. *Methods Enzymol* 276:307–326.
35. Adams PD, et al. (2011) The Phenix software for automated determination of macromolecular structures. *Methods* 55(1):94–106.
36. Jones TA, Zou J-Y, Cowan SW, Kjeldgaard M (1991) Improved methods for building protein models in electron density maps and the location of errors in these models. *Acta Crystallogr A* 47(Pt 2):110–119.
37. Emsley P, Lohkamp B, Scott WG, Cowtan K (2010) Features and development of Coot. *Acta Crystallogr D Biol Crystallogr* 66(Pt 4):486–501.
38. Davis IW, et al. (2007) MolProbity: All-atom contacts and structure validation for proteins and nucleic acids. *Nucleic Acids Res* 35(Web Server issue):W375–W383.
39. Baker NA, Sept D, Joseph S, Holst MJ, McCammon JA (2001) Electrostatics of nanosystems: Application to microtubules and the ribosome. *Proc Natl Acad Sci USA* 98(18):10037–10041.
40. Wyatt PJ (1997) Multiangle light scattering: The basic tool for macromolecular characterization. *Instrum Sci Technol* 25:1–18.
41. Karplus PA, Diederichs K (2012) Linking crystallographic model and data quality. *Science* 336(6084):1030–1033.

Supporting Information

Debler et al. 10.1073/pnas.1525783113

SI Methods

Peptide Substrates. Histone $H4^{1-21}$ (Ac-SGRGKGGKGLGKGGA-KRHRKV) and histone $H4^{1-21}$R3MMA (Ac-SGR[me]GKGGK-GLGKGGAKRHRKV) peptides were kind gifts from Heather Rust (The Scripps Research Institute, Jupiter, FL) and Paul Thompson (University of Massachusetts Medical School, Worcester, MA). The plasmid for expression of *Tb*RBP16 (UniProt: Q9XY40) was a kind gift from Laurie Read (SUNY Buffalo, Buffalo, NY).

Protein Expression and Purification. DNA fragments of *Tb*PRMT7 were amplified by PCR from genomic DNA, cloned into a pET28a vector (Novagen) containing an N-terminal PreScission protease (GE Healthcare) cleavable His_6-tag, overexpressed in *Escherichia coli* BL21-CodonPlus(DE3)-RIL cells (Stratagene), and grown in LB media containing appropriate antibiotics. Mutations in *Tb*PRMT7 were introduced by overlap extension PCR mutagenesis. Protein expression was induced at $OD_{600} \sim 0.6$ with 0.5 mM isopropyl-β-D-thiogalactoside at 18 °C for 16 h. The cells were harvested by centrifugation at 7,500 × *g* and 4 °C and lysed with a cell disrupter (Avestin) in a buffer containing 20 mM Tris, pH 8.0, 300 mM NaCl, 5 mM β-mercaptoethanol, 0.5 mM phenylmethylsulfonyl fluoride (Sigma), 2 μM bovine lung aprotinin (Sigma), and complete EDTA-free protease inhibitor mixture (Roche). After centrifugation at 35,000 × *g* for 45 min, the cleared lysate was loaded onto an Ni-NTA column (Qiagen) and eluted with an imidazole gradient. Protein-containing fractions were pooled, dialyzed against a buffer containing 20 mM Tris, pH 8.0, 100 mM NaCl, and 5 mM DTT, and subjected to cleavage with PreScission protease (GE Healthcare) for 12 h at 4 °C. After His_6-tag removal, the cleaved protein was bound to a heparin column (GE Healthcare) and eluted with an NaCl gradient. Protein-containing fractions were pooled, concentrated, and purified on a HiLoad Superdex 200 16/60 gel filtration column (GE Healthcare) in a buffer containing 20 mM Hepes, pH 7.5, 150 mM NaCl, and 0.5 mM Tris(2-carboxyethyl)phosphine (TCEP). His-tagged *Tb*RBP16 was expressed and purified as previously described (33), but the His-tag was removed.

Crystallization, Data Collection, Structure Determination, and Refinement. For formation of the complex with the AdoHcy, 20 mg/mL of purified *Tb*PRMT7 was mixed in a 1:2 molar ratio with AdoHcy and incubated for 1 h on ice. The crystallization solution consisted of 30% (wt/vol) PEG 400, 0.2 M $MgCl_2$, and 0.1 M Tris, pH 8.0. Crystals grew in space group $P3_221$ at room temperature within 2 wk. X-ray diffraction data were collected at the X29 beamline at the National Synchrotron Light Source (NSLS) at the Brookhaven National Laboratory. Diffraction data were processed in HKL2000 (34). The structure was solved by the single anomalous dispersion (SAD) phasing technique in the program AutoSol of the PHENIX package (35), using data obtained from seleno-L-methionine–labeled crystals. The asymmetric unit contained one dimer. Model building was performed in O (36) and Coot (37). The final model spanning residues 38–384 was refined in Phenix (35) to an R_{free} of 26.1% with excellent stereochemistry as assessed by MolProbity (38). Details for data collection and refinement statistics are summarized in Table S1. Figures were generated using PyMOL (Schrödinger, LLC), and the electrostatic potential was calculated with APBS (39). Atomic coordinates and structure factors have been deposited with the Protein Data Bank under PDB ID code 5EKU.

Multiangle Light Scattering. Purified proteins were characterized by multiangle light scattering after size-exclusion chromatography (40). Protein at 50 μM was injected onto a Superdex 200 10/300 GL size-exclusion chromatography column (GE Healthcare) equilibrated in a buffer containing 20 mM Hepes, pH 7.5, 150 mM NaCl, and 0.5 mM TCEP. The chromatography system was connected in series with an 18-angle light scattering detector (DAWN HELEOS) and refractive index detector (OptilabrEX) (Wyatt Technology). Data were collected every second at a flow rate of 0.25 mL/min at 25 °C. Data analysis was carried out using the program ASTRA, yielding the molar mass and mass distribution (polydispersity) of the sample.

Isothermal Titration Calorimetry. ITC measurements were performed at 15 °C using a MicroCal auto-iTC200 calorimeter (MicroCal, LLC). Protein was incubated with twofold molar excess of AdoHcy for 1 h at room temperature. Protein and peptide samples were then extensively dialyzed against a buffer containing 20 mM Hepes, pH 7.5, 20 mM NaCl, and 0.5 mM TCEP. Then, 2 μL of 1–4 mM peptide was injected into 0.2 mL of 0.1–0.4 mM protein in the chamber every 150 s. Baseline-corrected data were analyzed with ORIGIN software.

Amino Acid Analysis of Protein and Peptide Substrates. Unless otherwise described, 5 μg of the *Tb*RBP16 protein or 10 μM of the peptide substrates were methylated with 1.2 μg of WT *Tb*PRMT7 or the indicated amount of mutant *Tb*PRMT7 by incubating the mixture with 0.7 μM *S*-adenosyl-[*methyl*-^{3}H]-L-methionine ([*methyl*-^{3}H]-AdoMet) [stock solution of 7 μM (78.2 Ci/mmol; PerkinElmer Life Sciences) in 10 mM H_2SO_4/EtOH (9:1, vol/vol)] in 50 mM Hepes, pH 7.5, 100 mM NaCl, 1 mM DTT, and 5% (vol/vol) glycerol at 25 °C for 16 h in a total volume of 60 μL. When *Tb*RBP16 was used as the substrate, 60 μL of 25% (wt/vol) trichloroacetic acid and 20 μg of BSA were added to the reaction after completion, and the mixture was incubated at 25 °C for 30 min, followed by centrifugation at 4,000 × *g* for 30 min at 25 °C. The resulting pellet was washed with −20 °C acetone before acid hydrolysis. Alternatively, when peptides were used as substrates, the reactions were quenched with 4 μL of 25% (wt/vol) trichloroacetic acid. For reactions that were used for TLC, the peptides were purified via RP-HPLC. For reactions that were used for cation exchange chromatography, peptides were purified using OMIX C18 Zip-Tips with elution in 15 μL of trifluoroacetic acid/acetonitrile/water (0.1:50:50). In both cases, elution solvent was removed by vacuum centrifugation. Acid hydrolysis of all samples was performed with 50 μL of 6 M HCl at 110 °C for 20 h in vacuo. Once the acid was removed via vacuum centrifugation, the dried sample pellets were dissolved in 50 μL of water.

For samples analyzed by cation exchange chromatography, 1 μmol each of ω-MMA (acetate salt, M7033; Sigma), SDMA [di-(p-hydroxyazobenzene)-p-sulfonate salt, D0390; Sigma], and ADMA (hydrochloride salt; D4268; Sigma) were added as internal standards, and chromatography was then performed as previously described but using a buffer at pH 5.21 instead of 5.27 (10). The positions of the nonradioactive methylarginine standards were determined by detecting the absorbance of 50-μL fraction aliquots at 570 nm after being reacted with ninhydrin, and radioactivity of the remaining 950 μL from each fraction was determined through liquid scintillation, using the average of three 5- to 20-min counting cycles, as described (10). For samples analyzed by TLC, 10 μmol each of ω-MMA, SDMA, and ADMA were added to the peptide pellets. This mixture was dried via vacuum centrifugation and acid hydrolyzed as described

above. Then, 10 μmol of the three standards were also acid hydrolyzed individually and as a group. The dried hydrolysates were resuspended in 10 μL of water. Each reaction hydrolysate and individual standard hydrolysate was spotted onto silica plates (Polygram Sil G/UV$_{254}$, 805203; Macherey-Nagel) in 1-μL aliquots. Once the spots were dried, each plate was run in a 3:1 ethanol:water solvent mixture for about 8 h. After air drying, the plate was dipped momentarily in a ninhydrin solution [15 mg/mL ninhydrin dissolved in 97% (vol/vol) butanol, 3% (vol/vol) glacial acetic acid]. The plate was again allowed to air dry and then heated at 90 °C for 15 s. Visible ninhydrin spots were outlined, and the plate was sectioned into 5-mm-wide slices. The silica from each slice was mixed with 500 μL of water and vortexed for 2 h. This material was added to 5 mL of scintillation fluid to detect radioactivity using the average of three 20-min cycles.

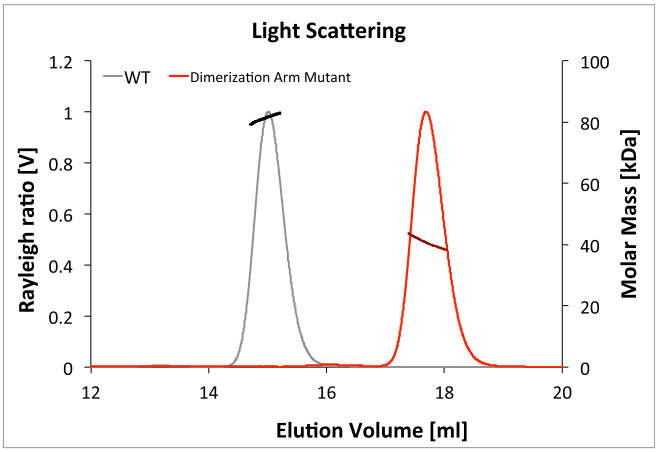

Fig. S1. Dimerization of *Tb*PRMT7. Molecular mass determination and Rayleigh ratio of WT *Tb*PRMT7 (light and dark gray, respectively) and of the dimerization arm mutant (light and dark red, respectively) by multiangle light scattering (MALS) coupled to size exclusion chromatography (Superdex 200 10/300 column; GE Healthcare). WT *Tb*PRMT7 forms a dimer whereas the dimerization arm mutant is monomeric.

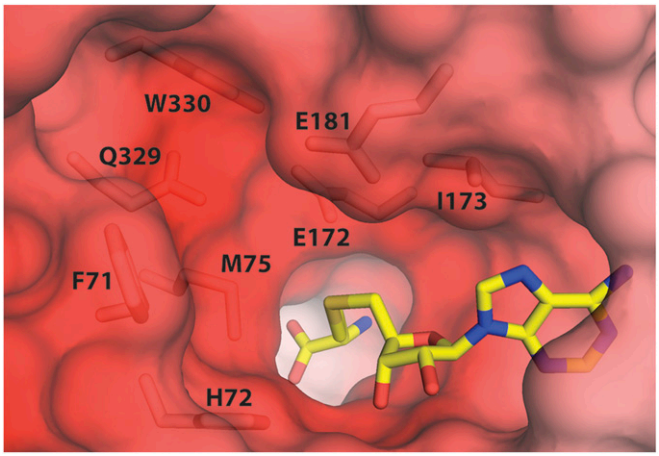

Fig. S2. Electrostatic surface potential of the active site shown between −20 kT/e (red) and +20kT/e (blue).

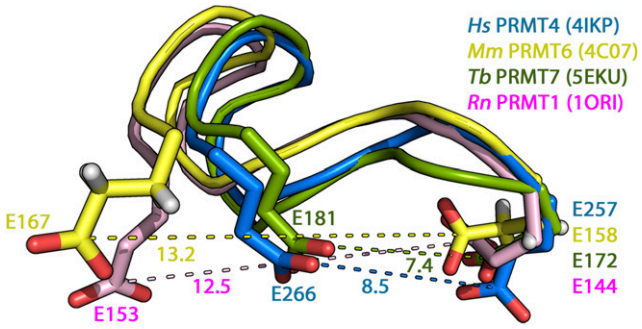

Fig. S3. *Tb*PRMT7's active site is generally smaller than that of type I enzymes. A structural alignment of the double E loops of *Tb*PRMT7 (PDB ID code 5EKU, chainA) and type I PRMTs with *Rn*PRMT1 (PDB ID code 1ORI, chainA), *Hs*PRMT4 (PDB 4IKP, chain A), and *Mm*PRMT6 (PDB 4C07, chain A) is shown with indicated coloring to match each E loop to its organism and enzyme. Distances between the glutamates of each E loop are given in Ångstöms. Dashed lines are colored to match the pairs of glutamate residues in each enzyme.

Table S1. Data collection and refinement statistics

Data collection	
Synchrotron	NSLS*
Beamline	X29
Space group	$P3_221$
Cell dimensions	
a, b, c, Å	a = b = 157.6, c = 97.4
α, β, γ, °	α = β = 90, γ = 120
Wavelength, Å	1.072
Resolution, Å†	50.0–2.80 (2.90–2.80)
No. of unique reflections	34,624 (3,417)
R_{sym}, %†	0.096 (88.6)
$CC_{1/2}$‡	0.997 (0.716)
$\langle I/\sigma I \rangle$†	12.1 (1.8)
Completeness, %†	100.0 (99.7)
Redundancy†	5.8 (5.8)
Refinement	
Resolution, Å	50.0–2.80
No. of reflections	34,586
Test set	3,380
R_{work}/R_{free}, %)	22.1/26.1
No. of atoms	5,564
rmsd	
Bond lengths, Å	0.004
Bond angles, °	0.9
⟨B-value⟩	
Protein, $Å^2$	80.0
AdoHcy, $Å^2$	110.1
MolProbity score/percentile	1.68/100
Ramachandran plot§	
Favored, %	96.33
Allowed, %	3.52
Outliers, %	0.15

*NSLS, National Synchrotron Light Source, Brookhaven National Laboratory.
†Highest-resolution shell is shown in parentheses.
‡$CC_{1/2}$, Pearson correlation coefficient between two random half-data sets (41).
§As determined by MolProbity.

Table S2. B-values of side-chain carboxyl groups from the glutamates of the double E loops in PRMTs indicate the first glutamate to be more rigid than the last one

	B-values (Å^2)					
	Carboxylate carbon		Carboxylate oxygens			
	CD		OE1		OE2	
Enzymes	First glutamate	Second glutamate	First glutamate	Second glutamate	First glutamate	Second glutamate
*Tb*PRMT7 (Type III, PDB 4M38)	23.84	29.06	22.19	36.35	27.89	33.01
*Mm*PRMT7 (Type III, PDB 4C4A)	37.39	46.01	40.03	47.35	25.11	47.83
*Ce*PRMT7 (Type III, PDB 3X0D)	51.31	98.59	54.21	87.5	52.8	104.58
*Rn*PRMT1 (Type I, PDB 1ORI)	46.41	54.71	46.7	54.98	48.97	57.55
*Rn*PRMT4 (Type I, PDB 3B3F)	33.2	37.81	31.63	41.91	34.66	38.35
*Mm*PRMT4 (Type I, PDB 2V7E)	40.67	44.13	41.76	44.47	39.65	44.44
*Hs*PRMT4 (Type I, PDB 4IKP)	37.45	37.69	38.11	38.29	37.28	38.34
*Hs*PRMT6 (Type I, PDB 4HC4)	29.46	46.09	30.96	48.51	39.56	49.09
*Mm*PRMT6 (Type I, PDB 4C07)	11.17	23.02	19.55	23.96	16.78	25.63
*Hs*PRMT5 (Type II, PDB 4GQB)	68.06	56.21	55.82	57.61	52.32	50.64

"First glutamate" and "Second glutamate" refer to the first and last glutamates in the double E loop, respectively. CD, OE1, and OE2 refer to the delta carbon and terminal epsilon oxygen atoms of the glutamates, respectively. *Ce*, *Caenorhabditis elegans*; *Hs*, *Homo sapiens*; *Mm*, *Mus musculus*; *Rn*, *Rattus norvegicus*; *Tb*, *Trypanosoma brucei*.

Table S3. Summary of ITC results

Protein	Peptide	[NaCl], mM	K_D, μM	ΔH, kcal/mol	N	ΔS, cal mol^{-1}K^{-1}
WT	H4$^{1-21}$	20	2.7 ± 0.2	3.59 ± 0.03	1.00 ± 0.01	37.9
WT	H4$^{1-21}$	150	50 ± 3	1.41 ± 0.03	1.00 ± 0.02	24.6
WT	H4$^{1-21}$	300	400,000	n/a	1.00 (fixed)	n/a
WT	H4$^{1-21}$	500	No binding	n/a	n/a	n/a
WT	H4$^{1-21}$R3MMA	20	9.1 ± 0.3	4.70 ± 0.02	1.00 ± 0.01	39.4
Glu181Asp mutant	H4$^{1-21}$	20	2.03 ± 0.05	5.52 ± 0.01	1.00 ± 0.01	45.2
Glu181Asp mutant	H4$^{1-21}$R3MMA	20	1.50 ± 0.03	5.55 ± 0.01	0.99 ± 0.01	45.9

The dissociation constant (K_D), binding enthalpy (ΔH), and the stoichiometry (N) were derived by curve fitting using a single-site model whereas the entropy (ΔS) was calculated from these values. n/a, not applicable.